An Advanced System to Monitor the 3D Structure of Diffuse Volcanic Ash Clouds

Jean-Paul Vernier, T. D. Fairlie, J. J. Murray, A. Tupper, C. Trepte, D. Winker, Jacques Pelon, Anne Garnier, Julien Jumelet, M. Pavolonis, et al.

An Advanced System to Monitor the 3D Structure of Diffuse Volcanic Ash Clouds

J.-P. VERNIER,*,+ T. D. FAIRLIE,+ J. J. MURRAY,+ A. TUPPER,# C. TREPTE,+ D. WINKER,+ J. PELON,@ A. GARNIER,*,+,@ J. JUMELET,@ M. PAVOLONIS,& A. H. OMAR,+ AND K. A. POWELL+

* *Science Systems and Applications, Inc., Hampton, Virginia*
+ *NASA Langley Research Center, Hampton, Virginia*
# *Australian Bureau of Meteorology, Northern Territory Regional Office, Casuarina, Northern Territory, Australia*
@ *Laboratoire Atmosphères, Milieux, Observations Spatiales, CNRS–INSU, Université de Versailles St. Quentin, Université de Paris 6, Paris, France*
& *NOAA/National Environmental Satellite, Data, and Information Service, Madison, Wisconsin*

(Manuscript received 3 October 2012, in final form 18 April 2013)

ABSTRACT

Major disruptions of the aviation system from recent volcanic eruptions have intensified discussions about and increased the international consensus toward improving volcanic ash warnings. Central to making progress is to better discern low volcanic ash loadings and to describe the ash cloud structure more accurately in three-dimensional space and time. Here, dispersed volcanic ash observed by the *Cloud–Aerosol Lidar and Infrared Pathfinder Satellite Observations (CALIPSO)* space-based lidar near 20 000–40 000 ft [~(6–13) km] over Australia and New Zealand during June 2011 is studied. This ash event took place 3 weeks after the Puyehue-Cordon Caulle eruption, which disrupted air traffic in much of the Southern Hemisphere. The volcanic ash layers are shown to exhibit color ratios (1064/532 nm) near 0.5, significantly lower than unity, as is observed with ice. Those optical properties are used to develop an ash detection algorithm. A ''trajectory mapping'' technique is then demonstrated wherein ash cloud observations are ingested into a Lagrangian model and used to construct ash dispersion maps and cross sections. Comparisons of the model results with independent observations suggest that the model successfully reproduces the 3D structure of volcanic ash clouds. This technique has a potential operational application in providing important additional information to worldwide volcanic ash advisory centers.

1. Introduction

Between April and May 2010, more than 100 000 flights were grounded at European airports, resulting in the loss of billions of euros for aviation companies and their customers. The decision to close vast parts of the European airspace was made in accordance with a widely accepted no-tolerance policy for the presence of volcanic ash in air corridors, after the relatively minor, but spatially and temporally extensive, eruption of the Icelandic volcano, Eyjafjallajökull (Sanderson 2010; see also the special issue of *Atmospheric Chemistry and Physics*, Vol. 10: http://www.atmos-chem-phys.net/special_issue212.html). This event highlighted weaknesses in the current infrastructure for managing airspace for civil aviation following a volcanic eruption. A specific weakness was the lack of adequate monitoring and forecast capabilities to provide sufficiently accurate and timely analyses of diffuse volcanic ash clouds needed to guide decision makers as to where aircraft could safely fly. This event was particularly challenging because of the spatial heterogeneity of the ash cloud and its presence in the lower to midtroposphere in very dense airspace. We define here the term ''diffuse'' to mean relatively low ash concentration on the order of $10^{-3}\,\mathrm{g\,m^3}$, which is near the ''safe'' threshold of $0.2 \times 10^{-3}\,\mathrm{g\,m^3}$ employed by European aviation authorities after the Icelandic eruption.

The Eyjafjallajökull episode motivated the International Civil Aviation Organization (ICAO) to convene an International Volcanic Ash Task Force (IVATF) to highlight ways to improve the management of airspace contaminated by volcanic ash (ICAO 2011, 2012). Among the key IVATF outcomes was a call for a consistent,

Corresponding author address: Dr. Jean-Paul Vernier, Science Systems and Applications, Inc., 11 Langley Blvd., Hampton, VA 23666.
E-mail: jeanpaul.vernier@nasa.gov

DOI: 10.1175/JAMC-D-12-0279.1

evidence-based approach to monitoring, forecasting, and avoiding "visible or discernible ash," while continuing to research the effects on aircraft systems and turbine engines of volcanic ash composition, sulfate–ash mixing, and exposure time, particularly in diffuse volcanic ash clouds.

A joint U.S. government and industry effort named the Volcanic Ash Ingestion Propulsion Research (VIPR) project is now planned by the National Aeronautics and Space Administration (NASA), the U.S. Air Force, the U.S. Geological Survey, engine manufacturers, and other aircraft industry participants. The VIPR project will conduct a series of diffuse volcanic ash tests beginning in 2014 to evaluate the impact of diffuse volcanic ash on operating jet aircraft systems in the laboratory to identify tolerances for various ingestion thresholds. A series of other IVATF recommendations call for increased work in these areas, including lidar and satellite remote sensing techniques (ICAO 2011, 2012). Together, the outcomes and recommendations of these efforts will support a pressing operational need for the world's nine volcanic ash advisory centers (VAACs) to implement new and improved techniques to estimate volcanic ash cloud properties including thickness and concentration.

The accuracy of VAAC advisories relies on the skilled use of satellite, ground, and airborne observations together with volcanic plume dispersion models. These models [e.g., the Hybrid Single Particle Lagrangian Integrated Trajectory (HYSPLIT; Stunder et al. 2007), "FLEXPART" (Stohl et al. 2005), and the Numerical Atmospheric Dispersion Modeling Environment (NAME; Jones et al. 2007; Dacre et al. 2011)] employ relatively simple representations of aerosol transformation and loss processes, and rely on accurate representations of volcanic column height, vertical ash distribution, and total injected mass at the source. Inverse methods have been used with infrared satellite retrievals to improve the initial conditions for plume dispersion models (Stohl et al. 2011). However, the initial conditions for these models remain largely uncertain. Consequently, such models often provide useful qualitative information about the volcanic ash distribution in the short term, but lack accurate information about volcanic cloud concentration, layering, and long-term dispersion (NOAA 2010). Geostationary (GEO) and low-Earth-orbit (LEO) satellites also provide geographic information for opaque and semitransparent volcanic ash clouds (Ellrod 2004; Gangale et al. 2010; Pavolonis et al. 2006; Pavolonis 2010; Prata 1989a,b; Prata and Prata 2012). Most remote sensing instruments currently used on board GEO and LEO satellites are equipped with passive nadir imagers (e.g., Geostationary Operational Environmental Satellite or Meteosat) or hyperspectral radiometers from ultraviolet to infrared wavelengths [e.g., Ozone Monitoring Instrument (OMI) on *Aura*, Atmospheric Infrared Sounder (AIRS) on *Aqua*, and Infrared Atmospheric Sounding Interferometer (IASI) on the *Meteorological Operation-A* and *-B* (*MetOp-A* and *-B*) satellites; see Clarisse et al. 2012; Carn et al. 2009; Karagulian et al. 2010; Klüser et al. 2013)].

The *Cloud Aerosol–Lidar and Infrared Pathfinder Satellite Observation* (*CALIPSO*) satellite, a collaboration between NASA and the Centre National d'Études Spatiale (CNES), has provided an unprecedented 3D view of aerosol and cloud layers in the atmosphere since 2006 (Winker et al. 2010) and is particularly effective in detecting and determining the altitude of volcanic plumes (Vernier et al. 2009; Vernier and Jumelet 2011; Winker et al. 2012). In this study, we show how trajectory mapping of *CALIPSO* observations offers a potential new capability to improve forecasts of diffuse volcanic ash. To demonstrate the feasibility of the method, we focus on volcanic eruption of Puyehue-Cordón Caulle, in Chile, during June 2011, which disrupted air traffic throughout much of the Southern Hemisphere due to the long-term presence of ash in the upper troposphere (6–14 km) and its multiple circumnavigations of the southern latitudes (Smithsonian Institution 2012).

In section 2, we provide a brief description of the *CALIPSO* mission and its ability to detect volcanic ash through measured optical parameters such as backscatter, depolarization, and color ratio. In section 3, we focus on the trajectory-mapping technique developed to map *CALIPSO* nighttime observations of volcanic ash clouds from discontinuous two-dimensional curtains along orbit tracks to continuous three-dimensional space. The resulting analyses are compared with infrared maps from the Multifunctional Transport Satellite (MTSAT) when the plume crossed Australia–New Zealand airspace between 20 and 24 June 2011. In section 4, we validate the analyses using independent daytime *CALIPSO* observations of volcanic ash, which were excluded from the trajectory mapping. In section 5, we discuss the advantages and limitations of the system and its potential to improve aviation safety during future volcanic events.

2. CALIPSO detection of volcanic ash clouds

The primary instruments on the *CALIPSO* payload are the Cloud–Aerosol Lidar with Orthogonal Polarization (CALIOP), which makes range-resolved measurements of elastic backscatter at 532 and 1064 nm and of linear depolarization at 532 nm, and the Imaging Infrared Radiometer (IIR), which contains three

medium-resolution spectral bands at 8.65, 10.6, and 12.05 μm. After 6 yr of nearly continuous observations (Winker et al. 2010), studies of several volcanic plumes in the upper-troposphere–lower-stratosphere (UTLS) region have shown that depolarization ratios (the ratio between the 532-nm perpendicular and parallel backscatter) and color ratios (the ratio between 1064- and 532-nm backscatter) provide information about particle shape and size, which is potentially useful in distinguishing among volcanic ash, sulfate aerosol layers, and ice clouds (Vernier et al. 2009; Winker et al. 2012). With a vertical resolution of 60 m up to 20-km altitude, CALIOP is particularly suitable for resolving ash cloud vertical layering.

Figure 1 shows nighttime curtains of the (a) CALIOP total attenuated backscatter at 532 nm (β'_{532}), (b) volume depolarization ratio (δ), and (c) attenuated color ratio (CR′, 1064/532 nm) between New Zealand and Australia around 1405 UTC on 23 June 2011.

Those quantities are defined according to the following equations:

$$\beta'_{532} = \beta'_{532.//} + \beta'_{532.\perp}, \quad (1)$$

$$\delta = \beta'_{532,\perp}/\beta'_{532,//}, \quad \text{and} \quad (2)$$

$$\mathrm{CR}' = \beta'_{532}/\beta'_{1064}, \quad (3)$$

where $\beta'_{532.//}$ and $\beta'_{532.\perp}$ are the parallel and perpendicular components of the total attenuated backscatter, respectively, and β'_{1064} is the total attenuated backscatter at 1064 nm.

The laminar multilayer features observed near 9–13 km that extend from 40° to 70°S exhibit a high volume depolarization ratio (0.3–0.4) but attenuated color ratios near 0.5, significantly lower than 1, as is typically found for ice clouds. In addition, Fig. 1d shows the 8.65 minus 12.05 μm and the 10.6 minus 12.05 μm brightness temperature differences (BTD) between the IIR channels. Positive BTDs identified over ocean indicate the presence of ice clouds (Dubuisson et al. 2008), whereas the presence of volcanic mineral material and gases (SO_2, H_2SO_4) results in negative BTDs due to their absorption properties in the IR (Pollack et al. 1973; Clarisse et al. 2010) and is particularly evident for Puyehue-Cordón Caulle (Klüser et al. 2013). Negative 10.6–12.05 and 8.65–12.05 BTDs in Fig. 1d are associated with layers having a low attenuated color ratio (Fig. 1c), which is consistent with the presence of a volcanic plume.

However, no recent volcanic eruption was reported in the study area. The culprit was a volcano located thousands of miles away that had erupted almost 3 weeks earlier. Indeed, a combined analysis of *CALIPSO* data and Moderate Resolution Imaging Spectroradiometer (MODIS) imagery obtained on 5 June 2011 indicated that the Puyehue-Cordón Caulle (Chile) volcano injected an ash cloud up to 14 km (NASA Observatory 2011) on 4 June 2011. The plume injected near the tropopause circumnavigated the world once (Klüser et al. 2013) before impacting Australia and New Zealand for a second time, between 20 and 24 June (Smithsonian Institution 2012). We note that during the first circumnavigation (6–14 June 2011), the CALIOP lidar was not operating because of a solar flare. After 14 June 2011, the signature of the Puyehue-Cordón Caulle volcanic plume was observed for several weeks near the tropopause in *CALIPSO* curtains similar to Fig. 1.

These observations led us to develop an ash detection algorithm based upon the CALIOP level 1 attenuated backscatter profiles obtained for the first month following the eruption. First, we averaged the data every 1° in latitude and 200 m vertically to increase the signal-to-noise ratio. We constructed a diffusion diagram (Fig. 2) of attenuated scattering ratio (SR′) versus attenuated color ratio (CR′). The ratio of total attenuated to molecular backscatter is SR′ defined as and is analogous to an optical aerosol mixing ratio of

$$\mathrm{SR}' = \beta'_{532}/\beta_m. \quad (4)$$

The molecular density β_m was calculated based on air density profiles from the Goddard Earth Observing System (GEOS-5) model, which are available within the CALIOP level 1 product. The SR′ and other backscatter coefficients were corrected for attenuation by molecular scattering and ozone absorption.

Theoretical calculations of CR′ for specific particulate color ratios are shown by the curves plotted in Fig. 2. The CR′ clusters of points are oriented toward the particulate color ratio isolines when SR′ increases, since the molecular backscatter becomes negligible. We then use the isoline 0.8 to separate data that are characteristic of volcanic materials from those that indicate ice clouds. The PDFs associated with SR′ values near 2, 3, and 5 are shown in Fig. 2 (bottom). While the method appears effective in separating ice from volcanic materials at SR′ greater than 2.5–3, separation is more problematic at lower levels, where the two Gaussian distributions of CR′ overlap each other. Low SR′ values are associated with relatively low ash concentrations. Using the same conversion factors from previous volcanic ash observations to derive ash mass concentration from lidar backscatter (Chazette et al. 2011; Winker et al. 2012), the detection limit using this technique for an SR′ near 3 would be around 75 μg m^{-3}. This is 26 times lower than

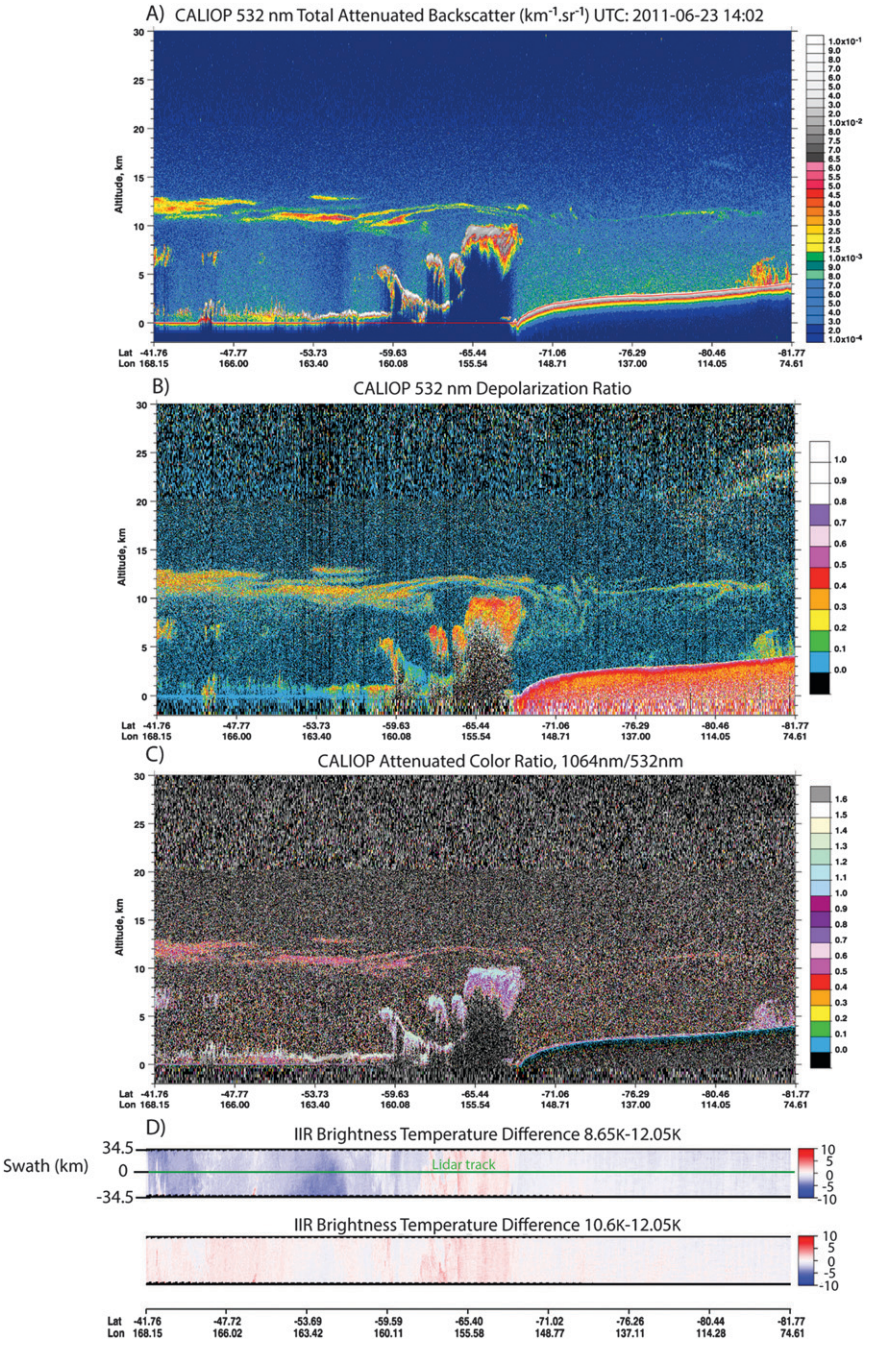

FIG. 1. Curtains of CALIOP level 1 data along an orbit track between Australia and New Zealand at 1335 UTC 23 Jun 2011: (a) 532-nm total attenuated backscatter, (b) 532-nm depolarization ratio, and (c) attenuated color ratio (1064/532). (d) BTDs (8.65 minus 12.05 μm and 10.6 minus 12.05 μm) from the IIIR on board *CALIPSO*.

the threshold limit of 2000 $\mu g\,m^{-3}$ defined after the Icelandic eruption, during which flights were allowed to operate.

After isolating CALIOP measurements contaminated by volcanic materials, we separate the ash from the sulfate contributions to the total attenuated backscatter, following Sugimoto and Lee (2006), Tesche et al. (2009), and Ansmann et al. (2011).

First, the particulate depolarization ratio (∂_t) was calculated from the volume depolarization ratio (∂) and

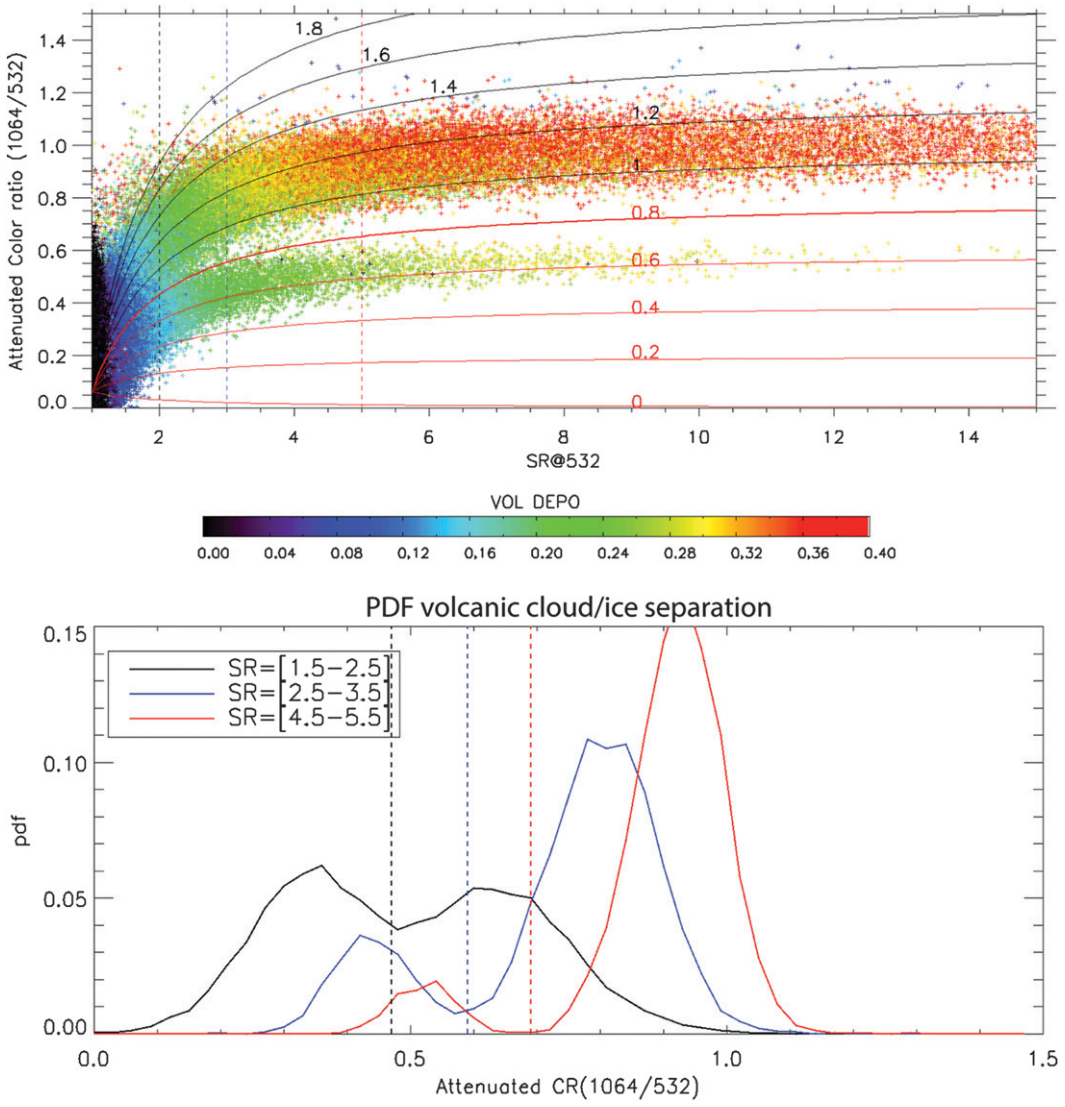

FIG. 2. (top) Diffusion diagram of attenuated scattering ratio (total attenuated backscatter–molecular backscatter) vs attenuated color ratio of all CALIOP measurements between 30° and 70°S and between 8 and 13 km during the first month after the Puyehue-Cordón Caulle eruption. Points are colored according to their volume depolarization. Theoretical color ratio curves for assumed particulate color ratios are also plotted. The isoline 0.8, which corresponds to the equation $y = (1/x)[0.8 \times (x - 1) + 1/16]$, is chosen to define the boundary, which separates ash and ice observations. (bottom) PDFs of attenuated color ratios for SR′ between 1.5 and 2.5 (black), 2.5 and 3.5 (blue), and 4.5 and 5.5 (red) to analyze separation criteria between volcanic cloud and ice.

SR′ following Cairo et al. (1999), according to Eq. (5) with $\partial_m = 0.0037$:

$$\partial_t = \frac{\mathrm{SR}' \times \partial \times (\partial_m + 1) - \partial_m \times (\partial + 1)}{\mathrm{SR}' \times (\partial_m + 1) - (\mathrm{SR}' + 1)}. \quad (5)$$

Knowing ∂_t and the theoretical ash ($\partial_{\mathrm{ta}} = 0.36$) and sulfate depolarization ratio ($\partial_s = 0.01$) (Ansmann et al. 2011), the ash-related backscatter β'_a and sulfate-related attenuated backscatter coefficients β'_s can be written as

$$\beta'_a = \beta'_t \frac{(\partial_t - \partial_s)(1 + \partial_a)}{(\partial_a - \partial_s)(1 + \partial_t)} \quad \text{and} \quad (6)$$

$$\beta'_s = \beta'_t - \beta'_a. \quad (7)$$

Figure 3 shows the ash and sulfate contributions to the total attenuated backscatter as a function of SR′. The sulfate-related attenuated backscatter represents less than 10% of the total attenuated backscatter, which indicates that the Puyehue-Cordón Caulle plume was

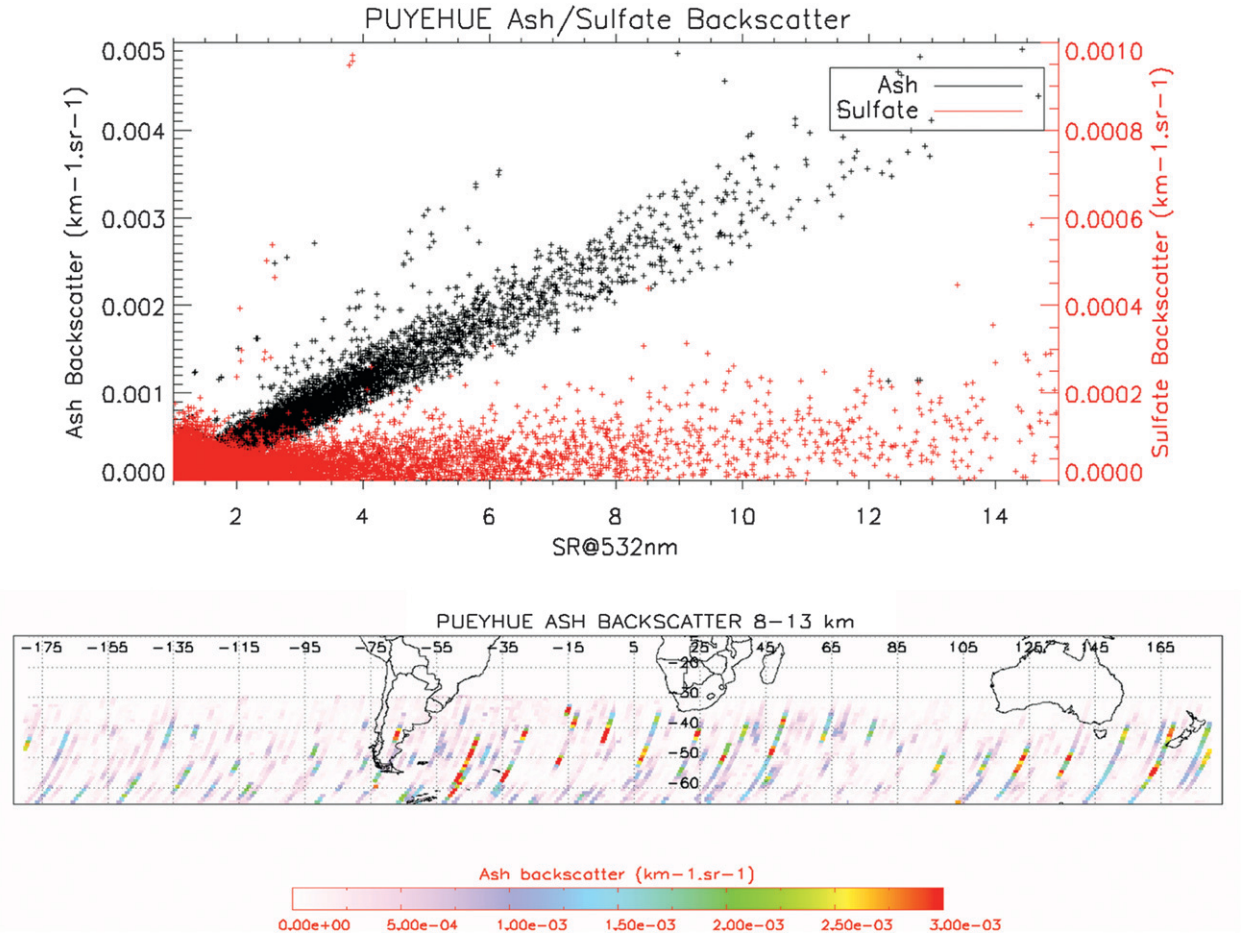

FIG. 3. (top) Diffusion diagram of ash and sulfate-related contributions to total attenuated backscatter vs attenuated scattering ratio for CALIOP observations identified as volcanic according to the separation criteria in Fig. 2. (bottom) Map of the 90th percentile of ash backscatter between 8 and 13 km assembled with those observations.

primarily made of ash. Simple calculations using previous conversion factors indicate that the ash mass concentration was still up to 550 $\mu g\,m^{-3}$ 10 days after the eruption. Note that the CALIOP backscatter coefficients may be underestimated since they are not corrected for attenuation due to any particle scattering from the plume itself or from cirrus clouds present above. However, since the volcanic plume was almost always near the tropopause above clouds, the attenuation from ice clouds has a minimal impact on β'_a. In the next generation of ash retrieval algorithms, however, the attenuation effect will be better evaluated by examining the CALIOP level 2 products.

Figure 3 (bottom) shows the corresponding map of the 90th percentile of ash backscatter between 8 and 13 km accumulated from CALIOP observations during the first month following the eruption. The 90th percentile refers to the highest 10% values of ash backscatter associated with measurements between 8 and 13 km along the CALIOP orbit track. The Puyehue-Cordón Caulle plume is seen almost everywhere in the Southern Hemisphere between 65° and 35°S, crossing major aircraft corridors between South America, South Africa, Australia, and New Zealand. All CALIOP observations of volcanic ash clouds seen on this map were used to initialize air parcel trajectories in a Lagrangian transport model.

3. Trajectory mapping of CALIPSO volcanic ash observations

Given the narrow swath of its lidar track (100 m), CALIOP alone lacks sufficient horizontal coverage to construct operationally useful wide-area maps of volcanic ash. We have used a Lagrangian trajectory model to map the *CALIPSO* data in 3D space and time, to obtain an advanced 3D view of volcanic ash in the UTLS, providing a means to monitor diffuse volcanic

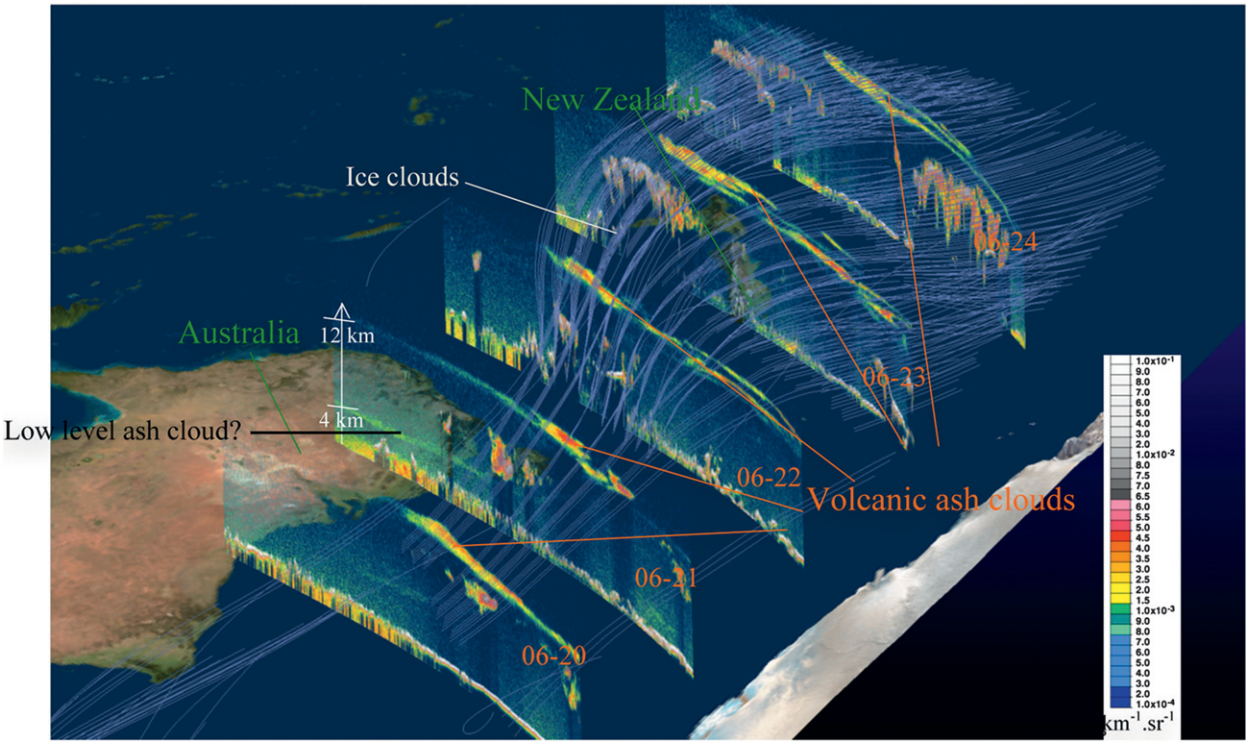

FIG. 4. Sequence of CALIOP 532-nm total attenuated backscatter curtains for 20–24 Jun 2011, depicting the passage of the Puyehue-Cordón Caulle volcanic ash cloud (yellow) near 8–12 km (20 000–40 000 ft) across a large area from north Antarctica to southeast Australia, Tasmania, and New Zealand. The blue lines between the curtains illustrate forward trajectories starting from the *CALIPSO* observations of the volcanic ash cloud.

ash clouds with high temporal, vertical, and horizontal resolution several weeks after an eruption.

Figure 4 shows a succession of curtains of CALIOP level 1 nighttime total attenuated backscatter for Australia and New Zealand from 20 to 24 June 2011. The coherent layers (yellow) observed near the tropopause [~(10–12) km] are associated with low color ratio (0.5, not shown) and were determined to be volcanic ash by the algorithm as described above. Blue lines in Fig. 4 show forward trajectories computed from the *CALIPSO* curtains. The 3D forward trajectories are computed using the NASA Langley Trajectory Model (LaTM; Pierce et al. 1997; Fairlie et al. 2009) and are driven by 6-h wind fields from the NASA GEOS-5.2 analyses (Rienecker et al. 2008). The LaTM uses a fourth-order Runge–Kutta method, with a 15-min time step. Note that the volcanic layers are linked by the trajectory paths, which provide a bridge between the separate orbital tracks. Note also that by 24 June, the trajectories have spread over an extensive region from New Zealand to Antarctica, as confirmed by *CALIPSO* observations on 24 June 2011.

We initialized air parcels at the location and time of the nighttime *CALIPSO* observations between 20° and 70°S and between altitudes of 8 and 14 km from 14 June 2011 and thereafter. The air parcels were initialized at intervals of 1° latitude and 200 m in the vertical. They were then tagged with a volcanic ash air parcel tracer obtained from the ash backscatter data that had been cleared of ice clouds. Instantaneous maps of ash backscatter were reconstructed from the accumulated air parcels, using a regular latitude–longitude grid of 1° × 1°, averaging air parcels younger than 10 days in each grid box with a time window of ±1 h.

Figure 5 shows maps of simulated ash backscatter (90th percentile of the ash backscatter values associated with air parcels between 8 and 13 km within a regular latitude–longitude grid of 1° × 1°) of the Puyehue-Cordón Caulle volcanic plume dispersion in the Southern Australian and New Zealand airspaces ~(26 000–43 000 ft/8–13) km] daily at 0000 UTC from 21 to 23 June (left). Model outputs are compared with collocated ash IR maps of 11–12-μm brightness temperature difference from MTSAT using the split-window technique (Prata 1989a,b). This method shows the volcanic ash cloud arriving from the Southern Ocean on 21 June 2011 associated with a trough of low pressure. The plume is passing above southeast Australia and the major cities of Melbourne and Sydney between 21 and 22 June, before

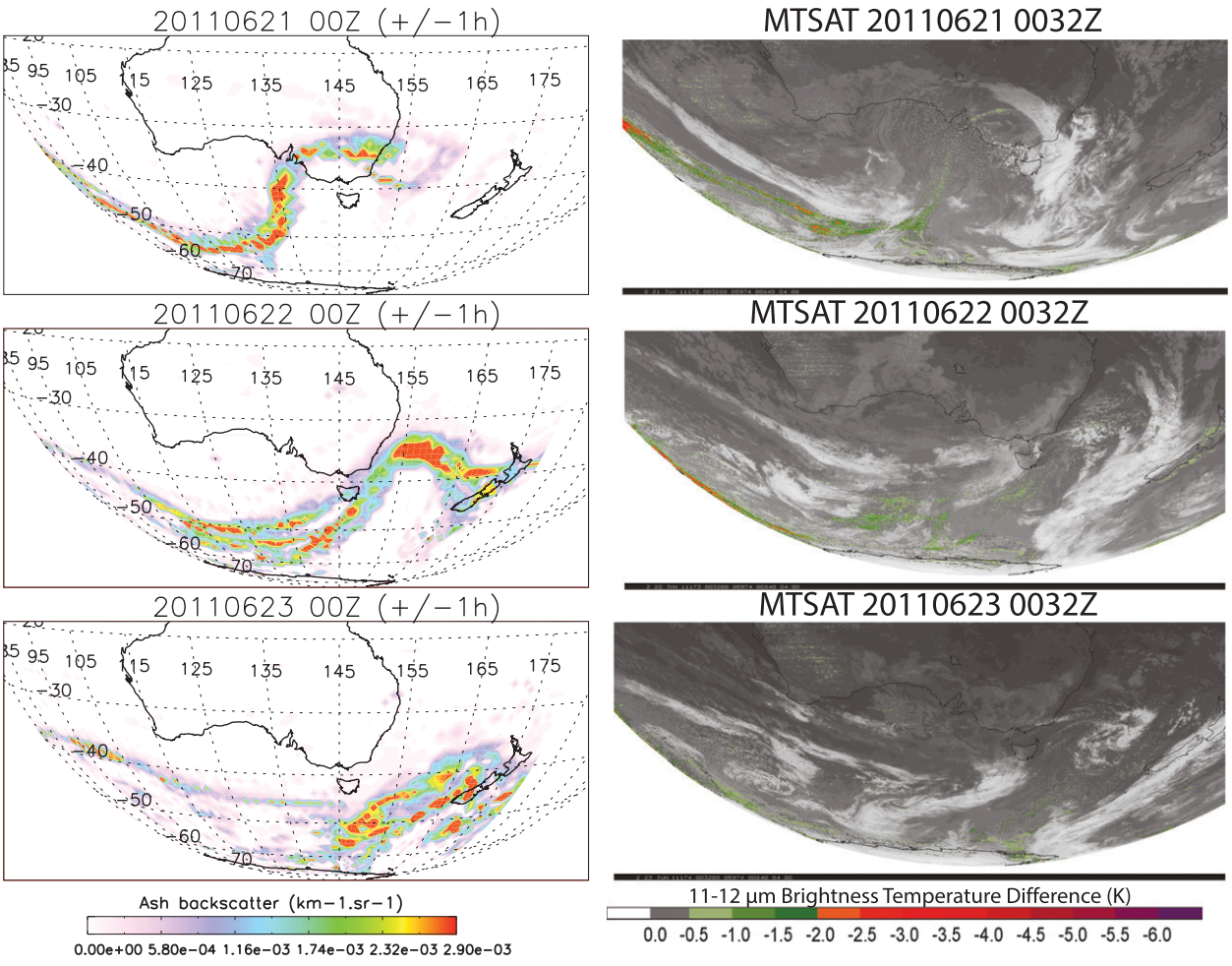

FIG. 5. (left) Maps of simulated ash backscatter (90th percentile) between 8 and 13 km [~(26 000–43 000) ft] at (from top to bottom) 0000 UTC 21–23 Jun 2011 with (right) the corresponding maps of 11–12-μm infrared BTDs from MTSAT using the split-window technique.

crossing the Tasman Sea and reaching New Zealand on 23 June. The model position of the plume on 21 June is confirmed by the corresponding IR map. Discontinuities in the plume can be seen in the IR maps afterward. Pieces of the plume are observed over the Southern Ocean, the Tasman Sea, and near New Zealand. Infrared observations of the plume over southeast Australia and the Tasman Sea were hindered by a strong frontal system with associated cloud rendering the detection of the ash cloud problematic. This was not a limitation for the ash backscatter trajectory maps. This demonstrates that the use of lidar observations coupled with trajectory model can provide useful information when ice clouds limit the retrieval of ash with IR techniques.

To verify the robustness of the trajectory-mapped volcanic ash 3D analyses, we use daytime *CALIPSO* lidar observations as an independent correlative dataset. Figure 6 shows simulated ash backscatter maps and cross sections, together with *CALIPSO* data on three daytime orbit tracks over Australia and New Zealand. Similar detection and retrieval criteria were applied to the *CALIPSO* daytime data as were applied to the nighttime data. Overall, Fig. 6 shows the transport of the Puyehue-Cordón Caulle volcanic plume across a large area encompassing Australia, the Tasman Sea, and New Zealand from 21 to 23 June 2011. Simulated ash backscatter cross sections reconstructed from the model along the *CALIPSO* tracks show features similar to those in the observations. They depict a volcanic ash cloud generally between 9- and 13-km altitude, extending within a relatively narrow corridor over Australia and the Tasman Sea on 21 and 22 June and then extending over a relative larger area including New Zealand on 23 June. In all figures, the vertical structure of the volcanic ash is well represented, but there are noticeable differences in intensity, especially on 22 June. There are several possible

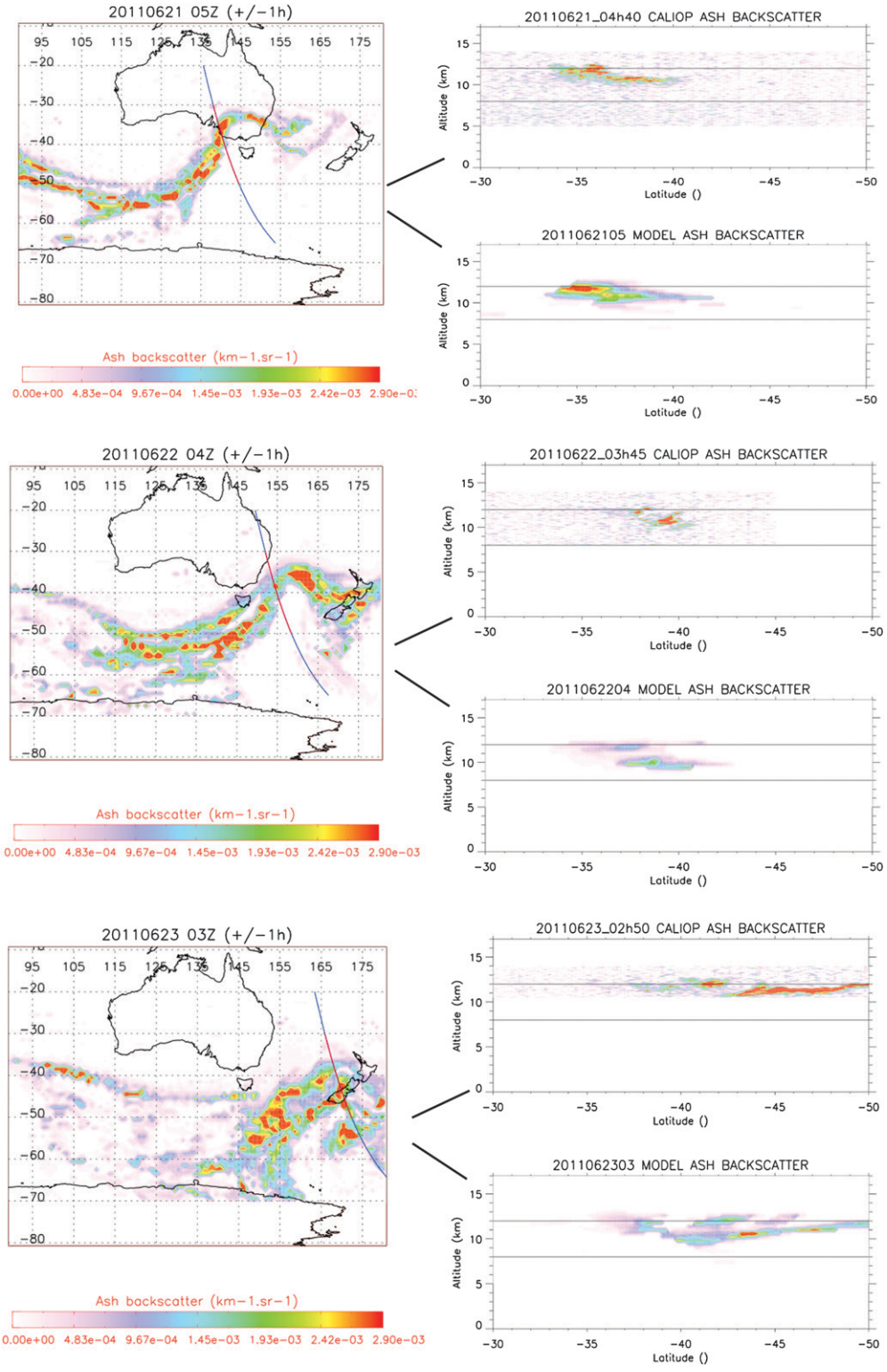

FIG. 6. (left) Maps of ash backscatter (90th percentile) between 8 and 13 km from the LaTM (top to bottom) at 0500 UTC 21 Jun, 0400 UTC 22 Jun, and 0300 UTC 23 Jun. Daytime *CALIPSO* track overpasses are displayed on the maps (colored lines). (right) Corresponding *CALIPSO* observed and modeled ash backscatter altitude–latitude profiles top and bottom panels, respectively, of each two panel set.

reasons for this: (i) the initial averaging of the *CALIPSO* nighttime data over 1°; (ii) the averaging of the model data 1° bins and 1-h time intervals, which could lead to an underestimate of ash backscatter if the plume is narrow; (iii) the mapped products depend on adequate sampling of the volcanic plume by the CALIOP lidar; and (iv) microphysical processes within the plume that are not explicitly represented in the model. A detailed investigation of the possible causes will be performed in the future.

4. Discussion

In contrast to the Eyjafjallajökull plume that extended over a smaller area in Europe, and in the lower and middle troposphere (see the special issue of *Atmospheric Chemistry and Physics*), the Puyehue-Cordón Caulle volcanic ash cloud was rapidly detrained in the higher-altitude air traffic corridors of the Southern Hemisphere midlatitudes by a strong westerly polar jet that prevailed near the tropopause. The ash cloud persisted at concentrations visible to pilots several weeks after the initial eruption.

The Darwin VAAC, which produces volcanic ash advisories for the airspace over Australia and the surrounding area, used standard VAAC practices to construct their ash advisories; this process consists of the qualitative and quantitative use of satellite data, model outputs, ground- and airborne-based in situ and remotely sensed observations, and air reports (ICAO 2011, 2012). However, long-term dispersion modeling of the Puyehue-Cordón Caulle plume, 3 weeks after the initial injection, was found not to be reliable due to insufficient initialization information for the diffuse plume. Thus, the Darwin VAAC was heavily dependent on fundamental satellite observations and first-order applications of the data. Infrared instrumentation from MODIS, the Advanced Very High Resolution Radiometer (AVHRR), and MTSAT (Fig. 5) were the primary sensors used to monitor the ash cloud (Tupper et al. 2004). In addition, the Darwin VAAC attempted to use information from the *CALIPSO* lidar near-real-time browse images to verify the vertical position of the ash cloud and run trajectories "manually." Figure 7 shows the quasi-real-time volcanic ash advisory maps (top), issued at 0000 UTC on 21 June 2011 by the Darwin VAAC (ftp://ftp.bom.gov.au/anon/gen/vaac/), as well as the collocated ash backscatter map produced by the trajectory-mapping technique. The ash analyses provided by the Darwin VAAC on 21 June (as shown), as well as on 22 and 23 June (not shown), are consistent with the model output on those days (Fig. 6). The model, however, provides additional information about the 3D structure of the volcanic plume, especially the extension of the plume's forward trajectory that was not available to the Darwin VAAC at the time of their advisories. For example, the model clearly shows the head of the volcanic ash cloud crossing the southern part of Australia east of the advisory box on 21 June. As was noted earlier, infrared observations of the plume at that longitude from the MTSAT GEO satellite were limited by a strong frontal system with associated cloud that rendered the detection of the plume problematic over the Tasman Sea. Without the accurate detection method for volcanic ash from *CALIPSO* observations developed in this study, and its combination with a trajectory-mapping method, estimating the speed of the ash transport by the Darwin VAAC was much more challenging and necessarily less accurate.

At low ash concentrations, much of the VAAC workload consisted of making judgment calls between potential ash and false alarms. The analysis was supplemented with experimental data shared through the community of volcanic cloud researchers, and with pilot reports obtained through aviation networks. The combination of *CALIPSO* observations of volcanic ash clouds and a Lagrangian trajectory model offers a potential new capability that VAACs could use to improve aviation safety worldwide.

As suggested by the comparison between daytime CALIOP observations and simulated analyses (Fig. 6), the trajectory-mapped ash product can be used to reconstruct cross sections of volcanic clouds in the UTLS along flight routes. Figure 8 shows such a cross section along a hypothetical flight route near the 37°S parallel, between Melbourne and Auckland, New Zealand (red line in Fig. 4). The simulated volcanic ash cloud depicted in Fig. 8 is located over the Tasman Sea between 9 and 12 km, well within the cruise level of commercial aircraft. If such a system were implemented for operational purposes, the reconstruction of ash cross sections along any flight routes could be used to optimize avoidance and rerouting options when flying during an elevated volcanic threat.

Criteria used to identify volcanic clouds using *CALIPSO* can also change from one eruption to another depending of the amount of sulfur dioxide injected in the initial eruptive column. The formation of sulfuric acid droplets from the conversion of SO_2 increases the load of spherical particles and consequently decreases the observed depolarization. The Puyehue-Cordón Caulle plume was shown to consist mainly of highly depolarized volcanic ash. However, other volcanic plumes (e.g., the Merapi plume; not shown) exhibited significantly lower depolarization consistent with volcanic materials composed of ash and liquid sulfate particles. Thus, the optical

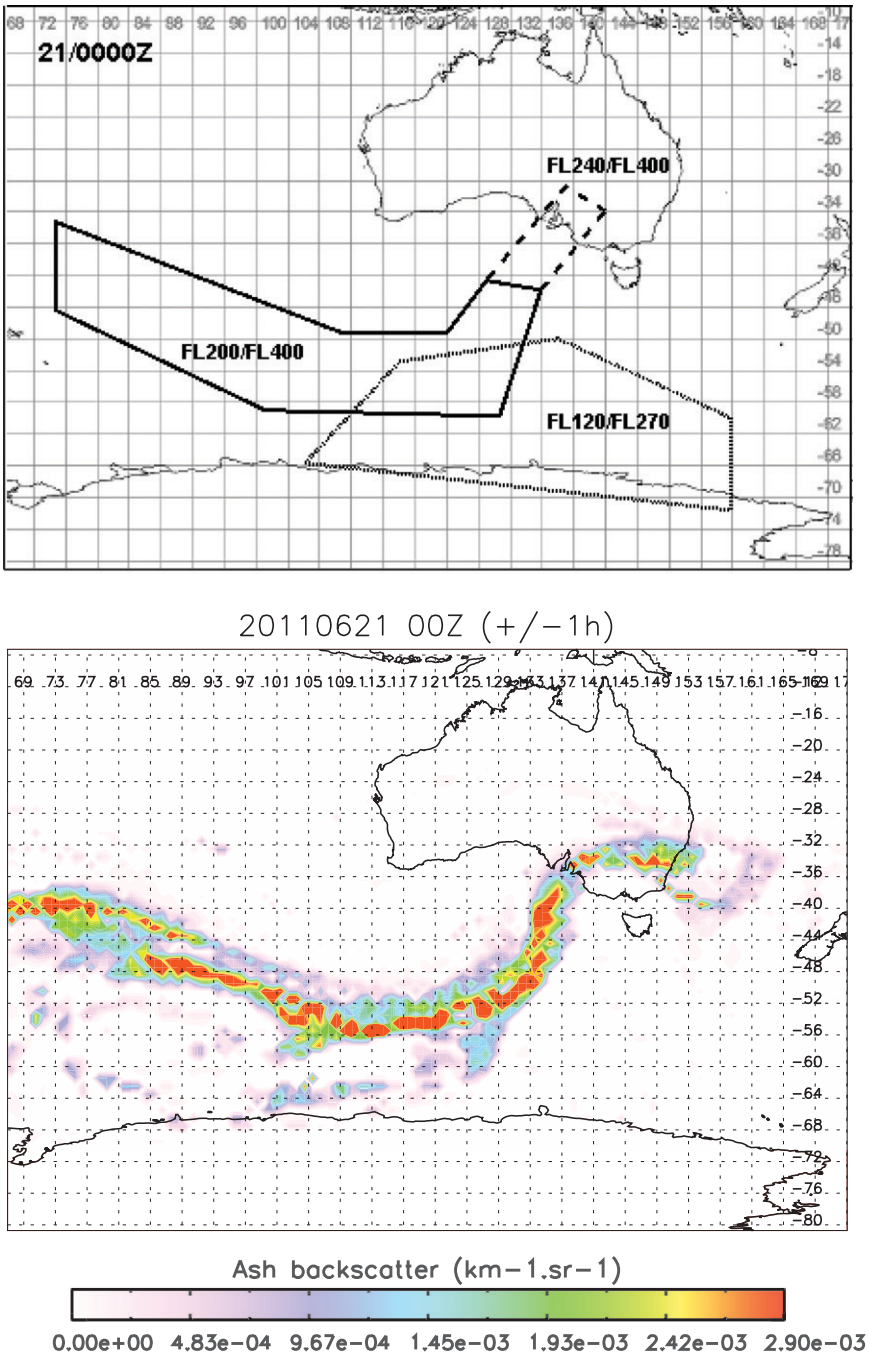

FIG. 7. (bottom) Map of simulated ash backscatter (90th percentile) between 8 and 13 km (26 000 and 43 000 ft) at 0000 UTC 21 Jun 2011 with (top) the corresponding near-real-time volcanic ash advisory issued by the Darwin VAAC at the same time.

parameters derived from *CALIPSO* can also be used to develop adapted algorithms that are able to distinguish mixtures of ash and sulfate.

It should also be noted that the use of spaceborne lidar technology to detect volcanic ash in the lower troposphere is limited under certain circumstances. During 21/22 June, pilots estimated that the ash layers extended as low as 20 000 ft over Australia (multiple height estimates were made, including at higher altitudes, but two pilots separately reported that they thought the ash they observed went that low). A *CALIPSO* overpass over Australia on the same day (Fig. 4, black arrow)

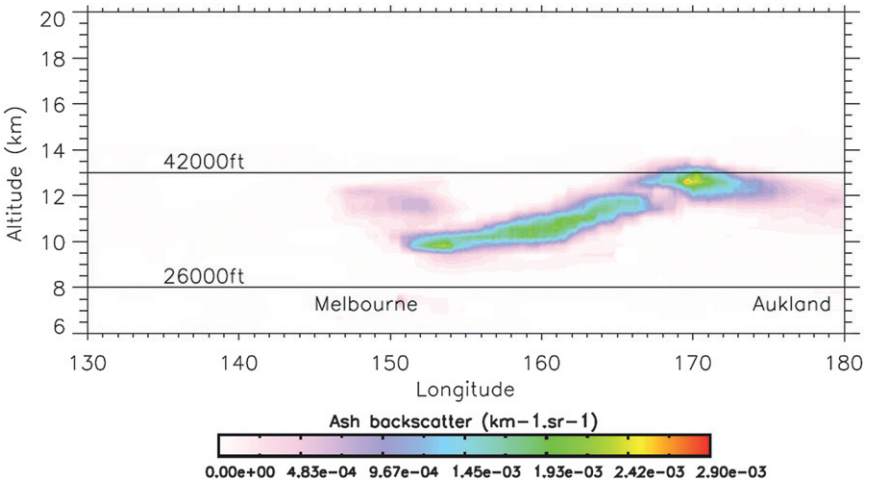

FIG. 8. Reconstructed ash backscatter cross section along the 37°S parallel (within 200 km) between Melbourne and Auckland at 0000 UTC 22 Jun 2011 when the Puyehue-Cordón Caulle ash cloud was crossing the Tasman Sea.

indicates a thin aerosol layer near 4–5 km that might correspond to those reports. Given the low altitude of this aerosol layer and its proximity to desert areas, we cannot exclude the possibility that this feature may be associated with a mineral dust layer, although the winter timing and moist soil conditions at the time would suggest that this as unlikely. Automatic detection of low-level ash clouds using only spaceborne lidar can be problematic since their optical signatures can be similar to tropospheric aerosols and especially mineral dust. In addition, they can be obscured and become undetectable when surmounted by optically thick clouds. Besides, ash particles are also potential ice nuclei, which can form cirrus in the upper troposphere that could potentially mask the nuclei's presence. In the future, the use of infrared information from the IIR on board CALIPSO will also be investigated to improve the differentiation between ice and ash and estimate mass loading.

5. Conclusions

We have presented a new system for monitoring the long-term dispersion of diffuse volcanic ash (or sulfate) clouds location in the UTLS, at levels between 20 000 and 40 000 ft (6–13 km), where most commercial and military air transport traffic at midlatitudes are concentrated. The trajectory mapping system we have illustrated is primarily based upon the detection of volcanic clouds via the analysis of their optical properties obtained from the *CALIPSO* lidar. The major result of this study is to show for the first time how observations from the *CALIPSO* lidar can be combined with a Lagrangian trajectory model to potentially improve the operational capability of the VAACs to monitor the 3D dispersion of volcanic ash clouds in the UTLS up to several weeks after an eruption. Due to the narrow swath of the CALIPSO lidar, the model needs adequate temporal and spatial sampling to be able to provide a good representation of the volcanic cloud. Despite this limitation, the system provides a potentially interesting source of diffuse ash information to the VAACs, since *CALIPSO* measurements can be obtained within 6–30 h after their acquisition through near-real-time products and give robust warning information in critical mass concentration regions. The technique does not rely necessarily on the most recent *CALIPSO* observations being available. Sensitivity tests have shown that even when eliminating up to 72 h of most recent nighttime observations, the model still reproduced the position and shape of the plume with good fidelity. Ash mass concentration has been obtained from lidar (Winker et al. 2012; Chazette et al. 2011) using in situ aircraft observations of the plume's mass loading to constrain the lidar retrieval. To do this entirely with satellites, we intend to explore incorporating complementary observations from the IIR (Garnier et al. 2012) in future work.

Using complementary passive satellite information, the CALIPSO-based system developed here could greatly assist the VAACs in obtaining timely information about the 3D structure of diffuse volcanic ash clouds. This information has the potential to improve aviation operations, passenger safety, and economic impacts during volcanic eruptions that disrupt aviation. Collaboration with VAAC operational agencies worldwide is the next logical step in implementing such a system for operational application, and this has begun.

Acknowledgments. The authors thank the *CALIPSO* team, and especially Z. Liu and M. Vaughan, for their advice on the use of the CALIOP data; K. Severance for his help in making Fig. 1; E. Ebert, M. K. Ko, and B. G. Doddridge for their review comments; and AirServices Australia for providing airspace routing information via their website (http://www.airservicesaustralia.com/).

REFERENCES

Ansmann, A., and Coauthors, 2011: Ash and fine-mode particle mass profiles from EARLINET-AERONET observations over central Europe after the eruptions of the Eyjafjallajökull volcano in 2010. *J. Geophys. Res.,* **116,** D00U02, doi:10.1029/2010JD015567.

Cairo, F., G. Di Donfrancesco, A. Adriani, L. Pulvirenti, and F. Fierli, 1999: Comparison of various linear depolarization parameters measured by lidar. *Appl. Opt.,* **38,** 4425–4432, doi:10.1364/AO.38.004425.

Carn, S. A., A. J. Krueger, N. A. Krotkov, K. Yang, and K. Evans, 2009: Tracking volcanic sulfur dioxide clouds for aviation hazard mitigation. *Nat. Hazards,* **51,** 325–343, doi:10.1007/s11069-008-9228-4.

Chazette, P., and Coauthors, 2011: Eyjafjallajökull ash concentrations derived from both lidar and modeling. *J. Geophys. Res.,* **117,** D00U14, doi:10.1029/2011JD015755.

Clarisse, L., F. Prata, J.-L. Lacour, D. Hurtmans, C. Clerbaux, and P.-F. Coheur, 2010: A correlation method for volcanic ash detection using hyperspectral infrared measurements. *Geophys. Res. Lett.,* **37,** L19806, doi:10.1029/2010GL044828.

——, D. Hurtmans, C. Clerbaux, J. Hadji-Lazaro, Y. Ngadi, and P.-F. Coheur, 2012: Retrieval of sulphur dioxide from the Infrared Atmospheric Sounding Interferometer (IASI). *Atmos. Meas. Tech.,* **5,** 581–594, doi:10.5194/amt-5-581-2012.

Dacre, H. F., and Coauthors, 2011: Evaluating the structure and magnitude of the ash plume during the initial phase of the 2010 Eyjafjallajökull eruption using lidar observations and NAME simulations. *J. Geophys. Res.,* **116,** D00U03, doi:10.1029/2011JD015608.

Dubuisson, P., V. Giraud, J. Pelon, B. Cadet, and P. Yang, 2008: Sensitivity of thermal infrared radiation at the top of the atmosphere and the surface to ice cloud microphysics. *J. Appl. Meteor. Climatol.,* **47,** 2545–2560.

Ellrod, G. P., 2004: Impact on volcanic ash detection caused by the loss of the 12 μm ''split window'' band on GOES Imagers. *J. Volcanol. Geotherm. Res.,* **135,** 91–103.

Fairlie, T. D., and Coauthors, 2009: Lagrangian sampling of 3-D air quality model results for regional transport contributions to sulfate aerosol concentrations at Baltimore, MD, in summer 2004. *Atmos. Environ.,* **43,** 3275–3288.

Gangale, G., A. J. Prata, and L. Clarisse, 2010: The infrared spectral signature of volcanic ash determined from high-spectral resolution satellite measurements. *Remote Sens. Environ.,* **114,** 414–425.

Garnier, A., J. Pelon, P. Dubuisson, M. Faivre, O. Chomette, N. Pascal, and D. P. Kratz, 2012: Retrieval of cloud properties using *CALIPSO* Imaging Infrared Radiometer. Part I: Effective emissivity and optical depth. *J. Appl. Meteor. Climatol.,* **51,** 1407–1425.

ICAO, 2011: Second Meeting of the International Volcanic Ash Task Force (IVATF/2). International Civil Aviation Organization IVATF/2-Rep. [Available online at http://www.icao.int/safety/meteorology/ivatf/MeetingMetaData/IVATF2FinalReport.pdf.]

——, 2012: Fourth Meeting of the International Volcanic Ash Task Force (IVATF/4). International Civil Aviation Organization IVATF/4-Rep. [Available online at http://www.icao.int/safety/meteorology/ivatf/MeetingMetaData/IVATF-4.FinalReport.pdf.]

Jones, A. R., D. J. Thomson, M. Hort, and B. Devenish, 2007: The U.K. Met Office's next-generation atmospheric dispersion model: NAME III. *Air Pollution Modeling and Its Application XVII,* C. Borrego and A.-L. Norman, Eds., Springer, 580–589.

Karagulian, F., L. Clarisse, C. Clerbaux, A. J. Prata, D. Hurtmans, and P. F. Coheur, 2010: Detection of volcanic SO_2, ash, and H_2SO_4 using the Infrared Atmospheric Sounding Interferometer (IASI). *J. Geophys. Res.,* **115,** D00L02, doi:10.1029/2009JD012786.

Klüser, L., T. Erbertseder, and J. Meyer-Arnek, 2013: Observation of volcanic ash from Puyehue-Cordón Caulle with IASI. *Atmos. Meas. Tech.,* **6,** 35–46, doi:10.5194/amt-6-35-2013.

NASA Observatory, cited 2011: Ash plume from Puyehue-Cordón Caulle. [Available online at http://earthobservatory.nasa.gov/IOTD/view.php?id=50954.]

NOAA, 2010: Science position paper on volcanic ash. NOAA Volcanic Ash Working Group Draft Science Position Paper, 22 pp. [Available online at http://svn.aviationweather.gov/vadma/images/0/05/NOAA_Position+Paper_on_Volcanic_Ash_06032010.pdf.]

Pavolonis, M. J., 2010: Advances in extracting cloud composition information from spaceborne infrared radiances—A robust alternative to brightness temperatures. Part I: Theory. *J. Appl. Meteor. Climatol.,* **49,** 1992–2012.

——, W. F. Feltz, A. K. Heidinger, and G. M. Gallina, 2006: A daytime complement to the reverse absorption technique for improved automated detection of volcanic ash. *J. Atmos. Oceanic Technol.,* **23,** 1422–1444.

Pierce, R. B., T. D. Fairlie, E. E. Remsberg, J. M. Russell, I. Il, and W. L. Grose, 1997: HALOE observations of the Arctic vortex during the 1997 spring: Horizontal structure in the lower stratosphere. *Geophys. Res. Lett.,* **24,** 2701–2704.

Pollack, J. B., O. B. Toon, and B. N. Khare, 1973: Optical properties of some terrestrial rocks and glasses. *Icarus,* **19,** 372–389.

Prata, A. J., 1989a: Observations of volcanic ash clouds in the 10-12 μm window using AVHRR/2 data. *Int. J. Remote Sens.,* **10,** 751–761.

——, 1989b: Radiative transfer calculations for volcanic ash clouds. *Geophys. Res. Lett.,* **16,** 1293–1296.

——, and A. T. Prata, 2012: Eyjafjallajökull volcanic ash concentrations determined using Spin Enhanced Visible and Infrared Imager measurements. *J. Geophys. Res.,* **117,** D00U23, doi:10.1029/2011JD016800.

Rienecker, M. M., and Coauthors, 2008: The GEOS-5 Data Assimilation System—Documentation of versions 5.01, 5.1.0, and 5.2.0. NASA/TM-2008-104606, NASA Tech. Rep. Series on Global Modeling and Data Assimilation, M. J. Suarez, Ed., Vol. 27, NASA Goddard Space Flight Center, 118 pp. [Available online at http://gmao.gsfc.nasa.gov/pubs/docs/GEOS5_104606-Vol27.pdf.]

Sanderson, K., 2010: Questions fly over ash-cloud models. *Nature,* **464,** 1253.

Smithsonian Institution, cited 2012: Puyehue-Cordón Caulle. Global Volcanism Program. [Available online at http://www.volcano.si.edu/world/volcano.cfm?vnum=1507-15=&volpage=var.]

Stohl, A., C. Forster, A. Frank, P. Seibert, and G. Wotawa, 2005: The Lagrangian particle dispersion model FLEXPART

version 6.2. *Atmos. Chem. Phys.,* **5,** 2461–2474, doi:10.5194/acp-5-2461-2005.

——, and Coauthors, 2011: Determination of time- and height-resolved volcanic ash emissions and their use for quantitative ash dispersion modeling: The 2010 Eyjafjallajokull eruption. *Atmos. Chem. Phys.,* **11,** 4333–4351.

Stunder, B. J. B., J. L. Heffter, and R. R. Draxler, 2007: Airborne volcanic ash forecast area reliability. *Wea. Forecasting,* **22,** 1132–1139.

Sugimoto, N., and C. H. Lee, 2006: Characteristics of dust aerosols inferred from lidar depolarization measurements at two wavelengths. *Appl. Opt.,* **45,** 7468–7474.

Tesche, M., A. Ansmann, D. Müller, D. Althausen, R. Engelmann, V. Freudenthaler, and S. Groß, 2009: Vertically resolved separation of dust and smoke over Cape Verde using multiwavelength Raman and polarization lidars during Saharan Mineral Dust Experiment 2008. *J. Geophys. Res.,* **114,** D13202, doi:10.1029/2009JD011862.

Tupper, A., S. Carn, J. Davey, Y. Kamada, R. Potts, F. Prata, and M. Tokuno, 2004: An evaluation of volcanic cloud detection techniques during recent significant eruptions in the western ''Ring of Fire.'' *Remote Sens. Environ.,* **91,** 27–46, doi:10.1016/j.rse.2004.02.004.

Vernier, J.-P., and J. Jumelet, 2011: Advances in forecasting volcanic plume evolution. *SPIE Newsroom,* 6 May, doi: 10.1117/2.1201103.003530.

——, and Coauthors, 2009: Tropical stratospheric aerosol layer from *CALIPSO* lidar observations. *J. Geophys. Res.,* **114,** D00H10, doi:10.1029/2009JD011946.

Winker, D. M., and Coauthors, 2010: The *CALIPSO* mission: A global 3D view of aerosols and clouds. *Bull. Amer. Meteor. Soc.,* **91,** 1211–1229.

——, Z. Liu, A. Omar, J. Tackett, and D. Fairlie, 2012: CALIOP observations of the transport of ash from the Eyjafjallajökull volcano in April 2010. *J. Geophys. Res.,* **117,** D00U15, doi:10.1029/2011JD016499.